Inorganic Chemistry

Article

pubs.acs.org/IC

Sm@C_{2v}(19138)-C_{76}: A Non-IPR Cage Stabilized by a Divalent Metal Ion

Yajuan Hao,[†] Lai Feng,*[,†] Wei Xu,[‡] Zhenggen Gu,[†] Ziqi Hu,[‡] Zujin Shi,*[,‡] Zdeněk Slanina,*[,§] and Filip Uhlík[∥]

[†]College of Physics, Optoelectronics and Energy & Collaborative Innovation Center of Suzhou Nano Science and Technology, Soochow University, Suzhou 215006, China

[‡]Beijing National Laboratory for Molecular Sciences, State Key Lab of Rare Earth Materials Chemistry and Applications, College of Chemistry and Molecular Engineering, Peking University, Beijing 100871, China

[§]Life Science Center of Tsukuba Advanced Research Alliance, University of Tsukuba, Tsukuba 305-8577, Japan

[∥]Department of Physical and Macromolecular Chemistry, Faculty of Science, Charles University in Prague, Albertov 6, Praha 2 128 43, Czech Republic

Supporting Information

ABSTRACT: Although a non-IPR fullerene cage is common for endohedral cluster fullerenes, it is very rare for conventional endofullerenes M@C_{2n}, probably because of the minimum geometry fit effect of the endohedral single metal ion. In this work, we report on a new non-IPR endofullerene Sm@C_{2v}(19138)-C_{76}, including its structural and electrochemical features. A combined study of single-crystal X-ray diffraction and DFT calculations not only elucidates the non-IPR cage structure of C_{2v}(19138)-C_{76} but also suggests that the endohedral Sm^{2+} ion prefers to reside along the C_2 cage axis and close to the fused pentagon unit in the cage framework, indicative of a significant metal−cage interaction, which alone can stabilize the non-IPR cage. Furthermore, electrochemical studies reveal the fully reversible redox behaviors and small electrochemical gap of Sm@C_{2v}(19138)-C_{76}, which are comparable to those of IPR species Sm@D_{3h}-C_{74}.

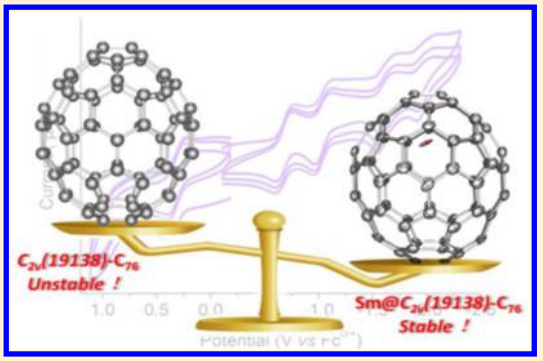

INTRODUCTION

Fullerene is a spherical carbon cage C_{2n} composed of 12 pentagons and a number of hexagons (i.e., $(2n - 20)/2$), which increases with the cage size.[1] The most typical fullerene C_{60} was discovered as early as 1985,[2] and the followed studies unambiguously revealed its I_h symmetry as well as the significant stability in air.[3] Noteworthy is that among the numerous C_{60} isomers only the I_h isomer can be obtained under ambient conditions. Structural characterization revealed that in the framework of I_h-C_{60} all 12 pentagons are isolated by hexagons. Later, such a topological feature has been approved to be common for all stable fullerenes and widely accepted as the isolated pentagon rule (IPR) for determining the stabilities of fullerene isomers.[4] In contrast, the non-IPR fullerenes that violate the IPR rule were proposed to have reduced stabilities relative to those of IPR isomers due to the enhanced local strain on the fused pentagons.[5] It was long believed that the non-IPR fullerenes had the least stabilities and could not survive in air.

However, in recent years, a number of non-IPR fullerenes have been emerging in the forms of fullerene derivatives (i.e., $C_{2n}Cl_x$, $C_{64}H_4$),[6] endohedrals,[7] or combinations.[8] For instance, in 2000 the first non-IPR fullerene $Sc_3N@D_3(6140)$-C_{68} was unambiguously characterized,[7a] demonstrating the improved stability of the non-IPR cage in the presence of endohedral metallic cluster. In fact, a huge number of non-IPR fullerenes are found to be available in topology, which challenges researchers to search for those that can survive in air. To date, more than 20 non-IPR endohedral metallofullerenes (EMFs) have been isolated and characterized by means of NMR, single-crystal XRD, or a combination.[9] In most cases, the non-IPR cage is stabilized by a metallic cluster (i.e., M_3N, M_2, Sc_2S; M = group 2 and 3 elements and most lanthanides). Echegoyen et al. recently proposed that not only the electron transfer between the cluster and the cage but also the geometry fit effect of the endohedral cluster contributes to the stabilization of the non-IPR cage.[10] However, as for conventional EMF M@C_{2n}, a non-IPR cage is very rare, probably because of the minimum geometry fit effect of the endohedral single metal ion. In particular, a non-IPR isomer La@C_{72} was identified in the form of La@C_2(10612)-C_{72}($C_6H_3Cl_2$).[8] It appears that both the endohedral La^{3+} ion and the exohedral derivatization contribute to the cage stabilization. Besides, other non-IPR M@C_{2n}, including Ca@C_2(10612)-C_{72}[11] and M@C_{76}

Received: December 5, 2014
Published: March 17, 2015

DOI: 10.1021/ic502911v
Inorg. Chem. 2015, 54, 4243−4248

(C_{2v}(19138) and C_1(17459), M = Yb, Ca, Sr, Ba),[12] were obtained only at the theoretical level. It is still unconfirmed whether a non-IPR cage can be stabilized by a single metal ion alone, and further experimental studies are very necessary. Herein, we report a non-IPR isomer of Sm@C_{76}, including structural characterization and electrochemical surveys. These studies experimentally demonstrate for the first time that the non-IPR cage can be stabilized by an endohedral divalent metal ion.

RESULTS AND DISCUSSION

The major isomer of Sm@C_{76} (i.e., Sm@C_{76}(I)) was prepared and isolated according to the previously reported procedure.[13] The sample purity was estimated to be higher than 95% based on chromatographic analysis (see Figure S1, Supporting Information). The composition of SmC_{76} was confirmed by MALDI-TOF mass (see Figure S2, Supporting Information). The UV−vis−NIR absorption spectrum of the sample is shown in Figure 1, which is consistent with the previous report.[13]

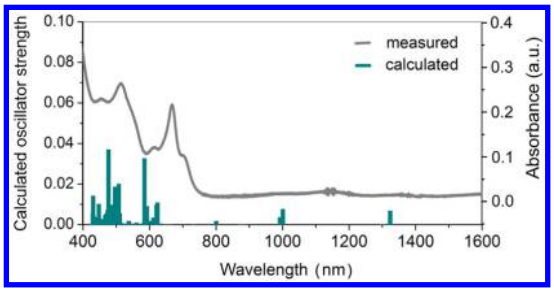

Figure 1. Measured and calculated UV−vis−NIR absorption spectra of Sm@C_{2v}(19138)-C_{76}.

Besides, the minor isomer of Sm@C_{76}(i.e., Sm@C_{76}(II)) was also observed, as suggested by the literature.[13] However, this isomer was not subjected to further characterization because of its lower yield.

A cocrystal of Sm@C_{76}/[Ni^{II}(OEP)] suitable for X-ray analysis was obtained by slow diffusion of a benzene solution of EMF into a $CHCl_3$ solution of [Ni^{II}(OEP)]. The molecular structure was resolved and refined in a monoclinic space group C_2. In the cocrystal, both the fullerene cage and the endohedral metal were found to be disordered. Specifically, two cage orientations have been identified with a ratio of 0.671:0.329. Figure 2 shows the major cage orientation, the major samarium site (Sm1, 0.376 occupancy), along with an adjacent [Ni^{II}(OEP)] moiety. The X-ray structure clearly shows a non-IPR cage of C_{2v}(19138)-C_{76} that is one of 19 151 possible non-IPR isomers for C_{76}. As can be seen clearly in Figure S3, Supporting Information, the C_2 axes of the two disordered cage orientations are similarly aligned relative to the porphyrin plane. Generally, the adjacent [Ni^{II}(OEP)] moiety is approaching the flat region of the C_{2v}(19138)-C_{76} cage, giving rise to the largest $\pi-\pi$ stacking between fullerene and the porphyrin moiety. The distances between the nickel ion in [Ni^{II}(OEP)] and the closest carbon ion in the major and minor cage orientations are 2.776 and 2.88 Å, respectively, similar to the values of 2.812 Å found in Sm@C_{2v}(3)-C_{80}·[Ni^{II}(OEP)][14] and 2.606 Å in Sm@C_{3h}-C_{74}·[Ni^{II}(OEP)],[15] suggesting similar interactions between Sm−fullerene and [Ni^{II}(OEP)].

Inside the fullerene cage, apart from the major Sm sites, four minor Sm sites with fractional occupancies ranging from 0.25 to 0.03 were detected. Figure 3 shows the major cage with all

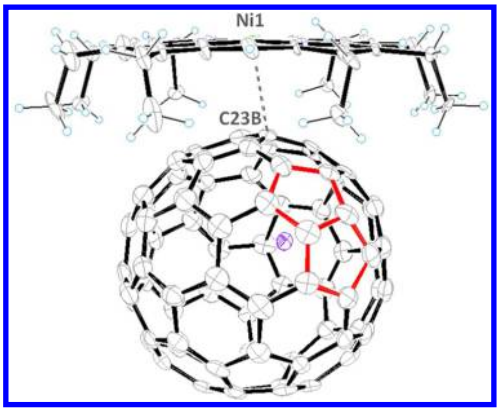

Figure 2. Ortep drawing of Sm@C_{2v}(19138)-C_{76}·[Ni^{II}(OEP)] with 25% thermal ellipsoids, showing the relationship between the fullerene cage and [Ni^{II}(OEP)]. Only the major cage orientation with 0.671 occupancy and the major Sm site (Sm1 with 0.376 occupancy) are shown, and the fused pentagons in the cage framework are highlighted in red. For clarity, the solvent molecules, minor cage orientation, and minor metal sites are omitted.

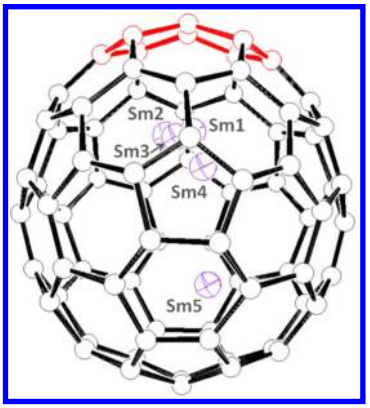

Figure 3. Drawing of Sm@C_{2v}(19138)-C_{76}, showing all of the samarium sites in the major cage orientation with 0.671 occupancy. Fused pentagons in the cage framework are highlighted by red. Occupancies of identified samarium sites are as follows: Sm1, 0.376(6); Sm2, 0.253(3); Sm3, 0.223(6); Sm4, 0.114(4); and Sm5, 0.034(3).

identified metal sites. Considering the major occupancy of the Sm1 site (0.376 occupancy), it is reasonable to assign the Sm1 site to the major cage orientation (0.671 occupancy). A closer look reveals that the Sm1 site resides slightly off the C_2 axis but is very close to the fused pentagons in the framework of C_{2v}(19138)-C_{76}. The shortest Sm−C distances in the major cage were determined in the range of 2.559−2.573 Å (see Table S1, Supporting Information). As for the minor metal sites Sm2 and Sm3 (0.253 and 0.223 occupancy), it is hard to determine which of the two sites corresponds to the minor cage orientation (0.325 occupancy). Nevertheless, either the Sm2 or the Sm3 site was found to be close to the fused pentagons in the framework of the minor cage. The shortest distances between cage carbons and Sm2 or Sm3 are similar to those between the major cage and Sm1 (see Table S1, Supporting Information). Therefore, the crystallographic data suggests that the samarium ion prefers to reside under the fused pentagons of C_{2v}(19138)-C_{76}, and the shortest Sm−C distances are comparable to those in Sm@C_2(5)-C_{82}[16] but shorter than the normal Sm−C bonding length (i.e., 2.8−3.0 Å) in some typical Sm complexes,[17] indicating the significant coordination

DOI: 10.1021/ic502911v
Inorg. Chem. 2015, 54, 4243−4248

interaction between the Sm^{2+} ion and the fused pentagons of C_{2v}(19138)-C_{76}. It has been found that such a feature is common for most non-IPR endohedral fullerenes.

To further shed light onto the structural and electronic feature of Sm@C_{2v}(19138)-C_{76}, DFT calculations were performed at the M06-2X/3-21G-SDD level[18] using the Gaussian 09 package.[19] The DFT-optimized Sm@C_{2v}(19138)-C_{76} structure is shown in Figure S4, Supporting Information. Inside the cage, the Sm^{2+} ion is residing along the C_2 axis and close to the fused pentagons, which is consistent with the XRD result. The shortest Sm−C distances in the optimized Sm@C_{2v}(19138)-C_{76} was revealed as 2.685 Å, slightly longer than that determined by X-ray analysis. Moreover, natural population analysis revealed that the Mulliken charge on the endohedral Sm atom is +2.037 e. This result may be interpreted as samarium donating two electrons to the fullerene cage, suggesting a formal electronic structure of $Sm^{2+}@(C_{76})^{2-}$. The Mulliken charges on cage carbons are plotted in Figure S4, Supporting Information. High charge densities are found for the fused pentagons and nearby carbons, indicative of strong ionic interactions between the endohedral metal and the fused pentagons.

Furthermore, the calculated molecular orbital diagrams are presented in Figure 4. As compared with those of empty

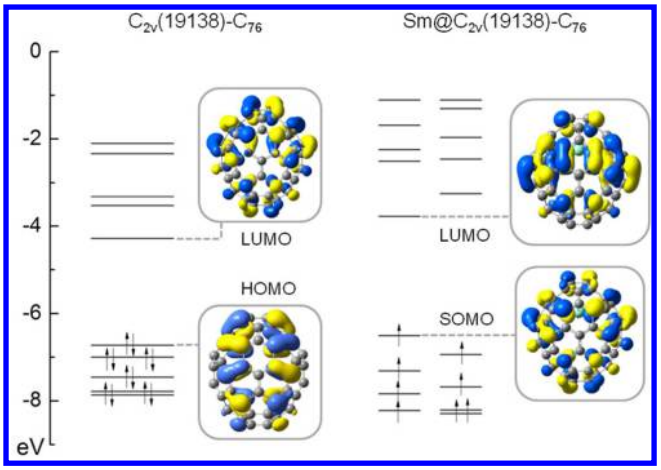

Figure 4. Molecular orbital diagrams for Sm@C_{2v}(19138)-C_{76} and C_{2v}(19138)-C_{76}. The empty fullerene C_{2v}(19138)-C_{76} was calculated with the geometry that it has in the endohedral fullerene. (Note: As an unrestricted M06-2X description is used for Sm@C_{2v}(19138)-C_{76}, just the alpha orbitals are shown. As for the beta orbitals, they are not shown for simplicity; their energy levels are not exactly the same as the alpha levels; however, they are close to them.) Insets show the SOMO (HOMO) and LUMO distributions of C_{2v}(19138)-C_{76} and Sm@C_{2v}(19138)-C_{76} at the DFT-M06-2X/3-21G~SDD level.

fullerene C_{2v}(19138)-C_{76}, the frontier orbitals (SOMO and LUMO) of Sm@C_{2v}(19138)-C_{76} are slightly shifted to higher energy levels, giving rise to a wider band gap of 2.74 eV relative to that of C_{2v}(19138)-C_{76} (2.45 eV). Calculations also reveal that both the SOMO and the LUMO of Sm@C_{2v}(19138)-C_{76} are mostly the cage orbitals with negligible contribution from the endohedral Sm^{2+} ion, which resemble those of most monometallofullerenes and indicate that the redox reactions take place mainly on the cage. In addition, it is also noteworthy that the SOMO distribution of Sm@C_{2v}(19138)-C_{76} is almost identical with the LUMO distribution of empty C_{2v}(19138)-C_{76}. Such a similarity might be accounted for by the proposal that the SOMO formation of Sm@C_{2v}(19138)-C_{76} is a direct result of filling the LUMO of C_{2v}(19138)-C_{76} by electron transfer from the endohedral Sm^{2+} ion. This proposal also facilitates understanding why there is no localization on the metal in the computed SOMO of Sm@C_{2v}(19138)-C_{76}.

The electronic spectrum of Sm@C_{2v}(19138)-C_{76} was calculated by means of time-dependent (TD) DFT at the B3LYP/3-21G~SDD level. As shown in Figure 1, the calculated absorption bands are presented mainly in the regions of 455−536 and 570−640 nm, composed of several sharp peaks. Such spectral features roughly resemble those of the measured spectrum of Sm@C_{76}(I) as well as the calculated results of Yb@C_{2v}(19138)-C_{76},[12a] despite the minor wavelength difference (i.e., ~100 nm). Considering these similarities, it is reasonable to conclude that Sm@C_{76}(I) possesses a cage of C_{2v}(19138)-C_{76}, which is consistent with our X-ray crystallographic result.

To further verify the superior availability of Sm@C_{2v}(19138)-C_{76} relative to other isomers (i.e., C_1(17459) and T_d(19151) isomers), relative energies of these isomers were calculated, though not at the same levels owing to convergency difficulties. In particular, C_{2v}(19138)-C_{76}, C_1(17459)-C_{76}, and T_d(19151)-C_{76} have been previously proposed to be the best hosts for Yb^{2+} and $(Lu_2)^{4+}$.[12a,20] Our calculation results reveal that the IPR species Sm@T_d(19151)-C_{76} is located 11.61 kcal mol^{-1} above Sm@C_{2v}(19138)-C_{76} at the M06-2X/3-21G~SDD level. The non-IPR isomer Sm@C_1(17459)-C_{76} comes 1.54 kcal mol^{-1} higher than Sm@C_{2v}(19138)-C_{76} at the B3LYP/6-311+G*~SDD level. Also, the SOMO−LUMO gap of the C_{2v}(19138) isomer was determined as 2.72 eV at the M06-2X/3-21G~SDD level, larger than 2.17 eV for the T_d(19151) isomer. At the B3LYP/6-311+G*~SDD level, though, the band gap of the C_{2v}(19138) isomer (i.e., 1.39 eV) is lower than 1.65 eV for C_1(17459). Overall, theoretical calculations predict the higher stability of Sm@C_{2v}(19138)-C_{76} relative to others, which is consistent with the higher production yield of Sm@C_{2v}(19138)-C_{76}. Note that these calculated relative stabilities of Sm@C_{76} isomers are very close to those reported for Yb@C_{76} isomers,[12a] suggesting the similar role of divalent metal ions in cage formation. The current studies also infer that the non-IPR M@C_{2n} can be more stable than the IPR analogue due to the strong metal−cage interactions.

Moreover, to better understand the superior stability of Sm@C_{2v}(19138)-C_{76}, a comparison study was performed between the non-IPR cage of C_{2v}(19138)-C_{76} and the well-known IPR cage of D_{3h}-C_{74},[14] because both are of similar size and can be stabilized by a Sm^{2+} ion in the form of Sm@C_{2n} (n = 37 or 38). The DFT-optimized Sm@C_{2v}(19138)-C_{76} and Sm@D_{3h}-C_{74} are presented in Figure 5. It is clearly seen that the two cages show very close geometrical similarity despite their different symmetries. The different cage motif is found at the pole of either cage, where a [5,5] bond is observed for C_{2v}(19138)-C_{76} but not for D_{3h}-C_{74}. Thus, as illustrated in Scheme 1, the cage of D_{3h}-C_{74} can be converted to C_{2v}(19138)-C_{76} by inserting a C_2 unit along the symmetric plane and the C_2 axis of the C_{74} cage, suggesting an unexpected structural correlation between the IPR and the non-IPR cages. It is also rational to propose that the similar cage structures of Sm@C_{2v}(19138)-C_{76} and Sm@D_{3h}-C_{74} are highly relevant to their superior stabilities relative to other isomers.

The electrochemical properties of Sm@C_{2v}(19138)-C_{76} were investigated by means of cyclic voltammogram (CV) and differential pulse voltammogram (DPV) studies. CV and DPV

DOI: 10.1021/ic502911v
Inorg. Chem. 2015, 54, 4243−4248

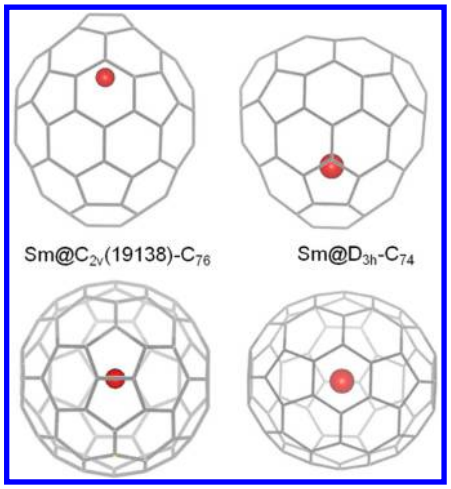

Figure 5. DFT-optimized structures of Sm@C_{2v}(19138)-C_{76} and Sm@D_{3h}-C_{74}: side views (up) and top views (down).

Scheme 1. Cage Motif Conversion via a C_2 Insertion (the C_2 unit is colored in blue)

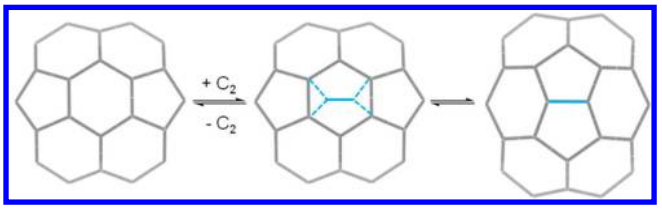

were recorded in *o*-dichlorobenzene (*o*-DCB) containing 0.05 M tetra(*n*-butyl)ammonium hexafluorophosphate ((*n*-Bu)$_4$NPF$_6$) as supporting electrolyte. All obtained redox potentials are summarized in Table 1 and compared with those of previously reported Sm−fullerenes. As shown in the CV profile (see Figure 6), Sm@C_{2v}(19138)-C_{76} exhibits four reversible one-electron reduction steps in the cathodic region but two reversible oxidation steps in the anodic region. In this respect, Sm@C_{2v}(19138)-C_{76} is very similar to most conventional endofullerenes and empty fullerenes, which usually show fully reversible redox behaviors.[21] Nevertheless, Sm@C_{2v}(19138)-C_{76} and other Sm−fullerenes show a major difference between their redox potentials. Specifically, the first oxidation potential of Sm@C_{2v}(19138)-C_{76} is 120 mV higher than that of Sm@D_{3h}-C_{74} but ca. 100 mV lower than those of middle-sized Sm−fullerenes (i.e., Sm@C_{3v}-C_{80} and Sm@C_2(5)-C_{82}),[14,15,16a] indicative of a moderate electron-donating ability. The first reduction potential of Sm@C_{2v}(19138)-C_{76} is 80−160 mV lower than those of previously reported Sm−fullerenes, suggesting a strong electron-accepting ability. All redox steps are also visible in the DPV profile (see Figure S5, Supporting Information), and their potential values are fully consistent with those obtained from CV. The electrochemical gap of Sm@C_{2v}(19138)-C_{76} is determined as 1.01 eV, similar to that of Sm@D_{3h}-C_{74} (0.97 eV)[14] but substantially smaller than those of middle-sized Sm−fullerenes (i.e., 1.28 eV for Sm@C_{2v}(3)-C_{80} and 1.26 eV for Sm@C_2(5)-C_{82}).[15,16] Therefore, the band gap of divalent M@C_{2n} might be mainly dependent on the cage size and cage structure rather than the IPR or non-IPR cage configuration.

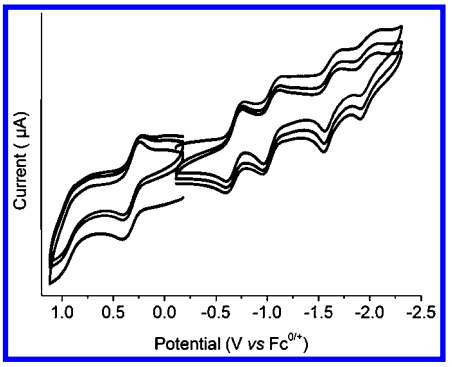

Figure 6. Cyclic voltammogram of Sm@C_{2v}(19138)-C_{76} in *o*-dichlorobenzene containing 0.05 M (*n*-Bu)$_4$NPF$_6$ (scan rate 100 mV s^{-1}).

CONCLUSIONS

In summary, a new non-IPR fullerene Sm@C_{2v}(19138)-C_{76} has been structurally characterized by a combined study of single-crystal XRD and DFT calculations. It was revealed that the endohedral Sm^{2+} ion prefers to reside along the C_2 cage axis and close to the fused pentagons in the framework of C_{2v}(19138)-C_{76}, suggesting significant metal−cage interaction, which alone can stabilize this non-IPR cage. Further investigations also suggested an unexpected structural correlation between the IPR and the non-IPR cages (i.e., D_{3h}-C_{74} and C_{2v}(19138)-C_{76}) as well as the larger band gap of Sm@C_{2v}(19138)-C_{76} relative to its IPR isomer (i.e., Sm@T_d(19151)-C_{76}). In addition, electrochemical investigations demonstrated the fully reversible redox behaviors of Sm@C_{2v}(19138)-C_{76}, which are similar to those of most IPR fullerenes.

EXPERIMENTAL SECTION

Synthesis and Isolation. The synthesis of Sm−metallofullerenes was described in earlier studies.[13] Briefly, Sm−metallofullerenes were produced using a modified arc-discharge method. Specifically, the anode graphite rod was filled with $SmNi_2$/graphite powder (1:10 atomic ratio), while a pure graphite rod was employed as the cathode. The arc discharge was carried out at 70 A with an electrode gap of ca. 1 cm under 400 Torr helium static atmosphere. Fullerene species were extracted from soot using *o*-xylene at high temperature under nitrogen atmosphere. The pure sample of Sm@C_{76}(I) was isolated and purified via a multistage HPLC procedure.

Table 1. Redox Potentials[a] (V vs $Fc^{0/+}$) of Sm@C_{2v}(19138)-C_{76} and Other Sm−Fullerenes

	$^{ox}E_2$	$^{ox}E_1$	$^{red}E_1$	$^{red}E_2$	$^{red}E_3$	$^{red}E_4$	EC gap
Sm@D_{3h}-C_{74}[c]	0.76	0.20	−0.77	−1.21	−1.72	−2.14	0.97
Sm@C_{2v}(19138)-C_{76}	0.95	0.32	−0.69	−1.04	−1.62	−1.97	1.01
Sm@C_{2v}(3)-C_{80}[d]	0.85[b]	0.43	−0.85	−1.23	−1.76	−2.07[b]	1.28
Sm@C_2(5)-C_{82}[e]		0.42[b]	−0.84	−1.01	−1.51	−1.90	1.26

[a]Half-wave potentials unless otherwise stated. [b]DPV values. [c]Data in ref 14. [d]Data in ref 15. [e]Data in ref 16a.

DOI: 10.1021/ic502911v
Inorg. Chem. 2015, 54, 4243−4248

Single-Crystal X-ray Diffraction Analysis. Black cocrystals of Sm@C_{76}/[Ni^{II}(OEP)] were obtained by allowing the benzene solution of fullerene and the chloroform solution of [Ni^{II}(OEP)] to diffuse together. X-ray data were collected at 90 K using a diffractometer (APEX II; Bruker Analytik GmbH) equipped with a CCD collector. Multiscan method was used for absorption correction. The structure was resolved using direct methods (SHELXS97) and refined on F^2 using full-matrix least-squares using SHELXL97.[22] Hydrogen atoms were added geometrically and refined with a riding model.

A cocrystal of Sm@C_{2v}(19138)-C_{76}·[Ni^{II}(OEP)]·0.86C_6H_6·0.14$CHCl_3$ contains another severely disordered lattice of C_6H_6 and $CHCl_3$ molecules that could not be modeled properly. Therefore, the program SQUEEZE, a part of the PLATON package of crystallographic software,[23] was used to calculate the solvent disorder area and remove its contribution from the intensity data.

Crystal data for Sm@C_{2v}(19138)-C_{76}·[Ni^{II}(OEP)]·0.86C_6H_6·0.14$CHCl_3$: C, 114.75; H, 46.75; Cl, 2; N, 4; Ni; Sm. M_r = 1761.27, 0.28 × 0.15 × 0.12 mm, monoclinic, C_2 (No.5), a = 25.339(11) Å, b = 14.944(6) Å, c = 19.147(8) Å, β = 93.844(5)°, V = 7234(5) Å^3, Z = 4, ρ_{calcd} = 1.617 g cm^{-3}, μ(Mo Kα) = 1.203 mm^{-1}, θ = 4.11−29.570°, T = 90 K, R_1 = 0.1326, wR_2 = 0.3076 for all data; R_1 = 0.1201, wR_2 = 0.2990 for 16 996 reflections ($I > 2.0\sigma(I)$) with 1456 parameters. Goodness of fit indicator 1.034. Maximum residual electron density 1.181 e Å^{-3}. More detailed crystal data are presented in Table S2,Supporting Information.

Electrochemistry. Differential pulse voltammetry (DPV) and cyclic voltammetry (CV) were carried out in *o*-dichlorobenzene (*o*-DCB) using a BAS CW-50 instrument. A conventional three-electrode cell consisting of a platinum working electrode, a platinum counter electrode, and a saturated calomel reference electrode (SCE) was used for both measurements. (n-Bu)$_4$NPF$_6$ (0.05 M) was used as the supporting electrolyte. All potentials were recorded against a SCE reference electrode and corrected against Fc/Fc$^+$. DPV and CV were measured at a scan rate of 20 and 100 mV s^{-1}, respectively.

Computational Method. All calculations were carried out using the Gaussian 09 program package.[19] Geometry optimizations and Mulliken population analysis were performed using density functional theory with the recently introduced M06-2X functional or B3LYP functional,[18a] 3-21G basis set[18b] for the C atom, and the SDD basis set[18c] (with the SDD effective core potential) for the Sm atom (the M06-2X/3-21G∼SDD level). The orbital energies were also calculated at a higher level (the M06-2X/6-311G*∼SDD level).

■ ASSOCIATED CONTENT

Supporting Information

HPLC, mass, and DPV profile of Sm@C_{2v}(19138)-C_{76}; coordinates and Mulliken charges of the DFT-optimized Sm@C_{2v}(19138)-C_{76}; X-ray crystallographic file in CIF format for Sm@C_{2v}(19138)-C_{76}·[Ni^{II}(OEP)]·0.86C_6H_6·0.14$CHCl_3$. This material is available free of charge via the Internet at http://pubs.acs.org.

■ AUTHOR INFORMATION

Corresponding Authors

*E-mail: fenglai@suda.edu.cn.
*E-mail: zjshi@pku.edu.cn.
*E-mail: zdenek@sals.natur.cuni.cz.

Notes

The authors declare no competing financial interest.

■ ACKNOWLEDGMENTS

This work was supported in part by the NSF of China (21171013, 51372158, 21471010), the Ministry of Science and Technology of China (Nos. 2013CB933402, 2011CB932601), the Jiangsu Specially Appointed Professor Program (SR10800113), the Project for Jiangsu Scientific and Technological Innovation Team (2013), and the Czech-Norwegian Research Program (7F14392). Also, we are grateful to Prof. T. Akasaka and Dr. M. Suzuki, University of Tsukuba, for their kind support in XRD measurements.

■ REFERENCES

(1) Fowler, P. W.; Manolopoulos, D. E. *An Atlas of Fullerenes*; Oxford Press: Clarendon, 1995.
(2) Kroto, H. W.; Heath, J. R.; O'Brien, S. C.; Curl, R. F.; Smalley, R. E. *Nature* **1985**, *318*, 162.
(3) Fowler, P. W.; Manolopoulos, D. E. *An Atlas of Fullerenes*; Oxford Press: Clarendon, 1995.
(4) Thilgen, C.; Diederich, F. *Chem. Rev.* **2006**, *106*, 5049.
(5) Kroto, H. W. *Nature* **1987**, *329*, 529.
(6) (a) Tan, Y. Z.; Xie, S. Y.; Huang, R. B.; Zheng, L. S. *Nat. Chem.* **2009**, *1*, 450. (b) Gao, C. L.; Li, X.; Tan, Y. Z.; Wu, X. Z.; Zhang, Q.; Xie, S. Y.; Huang, R. B. *Angew. Chem., Int. Ed.* **2014**, *53*, 7853. (c) Wang, C. R.; Shi, Z. Q.; Wan, L. J.; Lu, X.; Dunsch, L.; Shu, C. Y.; Tang, Y. L.; Shinahara, H. *J. Am. Chem. Soc.* **2006**, *128*, 6605.
(7) (a) Stevenson, S.; Fowler, P. W.; Heine, T.; Duchamp, J. C.; Rice, G.; Glass, T.; Harich, K.; Hajdu, E.; Bible, R.; Dorn, H. C. *Nature* **2000**, *408*, 427. (b) Yamada, M.; Kurihara, H.; Suzuki, M.; Guo, J. D.; Waelchli, M.; Olmstead, M. M.; Balch, A. L.; Nagase, S.; Maeda, Y.; Hasegawa, T.; Lu, X.; Akasaka, T. *J. Am. Chem. Soc.* **2014**, *136*, 7611.
(8) Wakahara, T.; Nikawa, H.; Kikuchi, T.; Nakahodo, T.; Rahman, G. M. A.; Tsuchiya, T.; Maeda, Y.; Akasaka, T.; Yoza, K.; Horn, E.; Yamamoto, K.; Mizorogi, N.; Slanina, Z.; Nagase, S. *J. Am. Chem. Soc.* **2006**, *128*, 14228.
(9) (a) Popov, A. A.; Yang, S. F.; Dunsch, L. *Chem. Rev.* **2013**, *113*, 5989. (b) Lu, X.; Feng, L.; Akasaka, T.; Nagase, S. *Chem. Soc. Rev.* **2012**, *41*, 7723.
(10) (a) Chen, N.; Mulet-Gas, M.; Li, Y. Y.; Stene, R. E.; Atherton, C. W.; Rodríguez-Fortea, A.; Poblet, J. M.; Echegoyen, L. *Chem. Sci.* **2013**, *4*, 180. (b) Mercado, B. Q.; Chen, N.; Rodríguez-Fortea, A.; Mackey, M. A.; Stevenson, S.; Echegoyen, L.; Poblet, J. M.; Olmstead, M. M.; Balch, A. L. *J. Am. Chem. Soc.* **2011**, *133*, 6752.
(11) Kobayashi, K.; Nagase, S. *J. Am. Chem. Soc.* **1997**, *119*, 12693.
(12) (a) Yang, T.; Zhao, X.; Xu, Q.; Zhou, C.; He, L.; Nagase, S. *J. Mater. Chem.* **2011**, *21*, 12206. (b) Yang, T.; Zhao, X.; Xu, Q.; Zheng, H.; Wang, W. W.; Li, S. T. *Dalton Trans.* **2012**, *41*, 5294.
(13) Okazaki, T.; Lian, Y.; Gu, Z.; Suenaga, K.; Shinohara, H. *Chem. Phys. Lett.* **2000**, *320*, 435.
(14) Xu, W.; Hao, Y.; Uhlik, F.; Shi, Z.; Slanina, Z.; Feng, L. *Nanoscale* **2013**, *5*, 10409.
(15) Xu, W.; Niu, B.; Shi, Z.; Lian, Y.; Feng, L. *Nanoscale* **2012**, *4*, 6876.
(16) (a) Xu, W.; Niu, B.; Feng, L.; Shi, Z.; Lian, Y. *Chem.—Eur. J.* **2012**, *18*, 14246. (b) Yang, H.; Jin, H.; Wang, X.; Liu, Z.; Yu, M.; Zhao, F.; Mercado, B. Q.; Olmstead, M. M.; Balch, A. L. *J. Am. Chem. Soc.* **2012**, *134*, 14127.
(17) (a) Woodman, T. J.; Schormann, M.; Hughes, D. L.; Bochmann, M. *Organometallics* **2003**, *22*, 3028. (b) Evans, W. J.; Clark, R. D.; Ansari, M. A.; Ziller, J. W. *J. Am. Chem. Soc.* **1998**, *120*, 9555.
(18) (a) Zhao, Y.; Truhlar, D. *Theor. Chem. Acc.* **2008**, *120*, 215. (b) Becke, A. D. *J. Chem. Phys.* **1993**, *98*, 5648. (c) Cao, X.; Dolg, M. *THEOCHEM* **2002**, *581*, 139.
(19) Frisch, M. J. et al. *Gaussian 09*, Revision A.02; Gaussian, Inc.: Wallingford, CT, 2009.

DOI: 10.1021/ic502911v
Inorg. Chem. 2015, 54, 4243−4248

(20) Umemoto, H.; Ohashi, K.; Inoue, T.; Fukui, N.; Sugai, T.; Shinohara, H. *Chem. Commun.* **2010**, *46*, 5653.
(21) Chaur, M. N.; Melin, F.; Ortiz, A. L.; Echegoyen, L. *Angew. Chem., Int. Ed.* **2009**, *48*, 7514.
(22) Sheldrick, G. *Acta Crystallogr., Sect. A* **2008**, *64*, 112.
(23) (a) Spek, A. L. *PLATON. A multipurpose crystallographic tool*; Utrecht University: The Netherlands, 2003. (b) SQUEEZE: van der Sluis, P.; Spek, A. L. *Acta Crystallogr., Sect. A* **1990**, *46*, 194.

DOI: 10.1021/ic502911v
Inorg. Chem. 2015, 54, 4243−4248